



Research Paper / Makale

The Role of Eu³⁺ Ion on Luminescence, TL Kinetic Parameters and Electrochemical Behaviors of Sr_{0,5}Ca_{0,5}WO₄ Phosphor Synthesized via Sol-Gel Technique

Mehmet İsmail KATI^{1a*}, İlker Çetin KESKİN^{2b}, Murat TÜREMİŞ^{3c}, Ahmet ÇETİN^{4d}, Rana KİBAR^{4e}

¹Experimental Science Applications and Research Center, Manisa Celal Bayar University, 45030 Manisa, Turkey

²Department of Electricity and Energy, Soma Vocational High School, Manisa Celal Bayar University, 45500 Manisa, Turkey

³Department of Physics, Faculty of Engineering and Natural Sciences, Bursa Technical University, Bursa, Turkey

⁴Department of Physic, Faculty of Science and Art, Manisa Celal Bayar University, 45030 Manisa, Turkey

mehmetismailkati@gmail.com

Received/Geliş: 29.11.2020

Accepted/Kabul: 03.01.2021

Abstract: The Eu³⁺ doped Sr_{0,5}Ca_{0,5}WO₄ has been synthesized by the sol-gel method for the first time. The phosphors were analyzed by XRD, SEM, DTA/TG optical absorption spectra, radioluminescence (RL), photoluminescence (PL), and thermoluminescence (TL) spectra. The energy transfer mechanism was determined on Eu³⁺ doped Sr_{0,5}Ca_{0,5}WO₄ phosphor. The XRD results reveal that the samples exhibit a tetragonal scheelite structure. FT-IR spectra provide the proof of scheelite structure with W-O anti-symmetric stretching vibration in [WO₄]²⁻ tetrahedrons at 750-910 cm⁻¹. The Sr_{0,5}Ca_{0,5}WO₄ phosphor showed a broad emission between 350-750 nm with a maximum of 506 nm. Sr_{0,5}Ca_{0,5}WO₄:0.5Eu³⁺ phosphor exhibit characteristic emissions of Eu⁺³ (545, 592, 614, 650, and 700 nm) in the RL spectrum. The host material has excellent energy transfer efficiency for lanthanide ions. The kinetic parameters were calculated by the computerized glow curve deconvolution (CGCD) analysis method. As a result of CGCD, three peaks (E_{trap}:0.74-1.46 eV) for un-doped Sr_{0,5}Ca_{0,5}WO₄ and five peaks (E_{trap}:0.75-1.28 eV) for Sr_{0,5}Ca_{0,5}WO₄:Eu³⁺ were determined under main TL glow curve. In the cyclic voltammogram of the doped sample, an oxidation peak of about -0.4 eV, which is thought to be derived from Eu³⁺, was observed. Based on the results, the Sr_{0,5}Ca_{0,5}WO₄:Eu⁺³ phosphors may be potential applicants for LEDs.

Key words : Kinetic parameters, luminescence, rare earth doping, sol-gel method

Sol-Jel Tekniği ile Sentezlenmiş Sr_{0,5}Ca_{0,5}WO₄ Fosforunda Eu³⁺ İyonunun Lüminesans, TL Kinetik Parametreler ve Elektrokimyasal Davranışındaki Rolü

Öz: Eu³⁺ katkılılandırılmış Sr_{0,5}Ca_{0,5}WO₄ sol-jel method ile ilk kez sentezlenmiştir. Fosforların DTA/TG, XRD, SEM, optik absorpsiyon, fotolüminesans (PL), radyolüminesans (RL) ve termolüminesans (TL) teknikleriyle analiz edilmiştir. Enerji transfer mekanizması Eu³⁺ katkılı fosfor için belirlenmiştir. XRD sonuçları örneklerin tetragonal şelit yapıda olduğu ortaya koymaktadır. RL spektrumlarında Sr_{0,5}Ca_{0,5}WO₄ fosforu 350-750 nm aralığında 506 nm zirve yapan geniş bir emisyon bandı göstermiştir ve Sr_{0,5}Ca_{0,5}WO₄:0.5Eu³⁺ fosforu Eu⁺³ iyonunun karakteristik (545, 592, 614, 650, and 700 nm) geçişlerini göstermiştir. Kinetik parametrelerin hesaplanmasında bilgisayarlı ışım eğrisi ayrıştırma (CGCD) metodu kullanılmıştır. CGCD sonuçları, ana TL ışım eğrilerinde Sr_{0,5}Ca_{0,5}WO₄ örneği için üç ve Sr_{0,5}Ca_{0,5}WO₄:Eu³⁺ fosforu için beş pik belirlenmiştir. Katkılılandırılmış örneğin döngüsel voltamogramında Eu³⁺ dan kaynaklandığı düşünülen yaklaşık -0.4 eV' lik bir oksidasyon zirvesi gözlemlendi. Bu sonuçlar temelinde Sr_{0,5}Ca_{0,5}WO₄:Eu⁺³ fosforları ışık yayan diyot uygulamaları için potansiyel oluşturabilirler.

Anahtar kelimeler: Kinetik parametreler, lüminesans, nadir toprak iyonu dopu, sol-jel metodu

How to cite this article

Kati, M. İ., Keskin, İ.Ç., Türemiş, M., Çetin, A., Kibar, R. "The Role of Eu³⁺ Ion on Luminescence, TL Kinetic Parameter and Electrochemical Behaviors of Sr_{0,5}Ca_{0,5}WO₄ Phosphor Synthesized via Sol-Gel Technique", El-Cezeri Journal of Science and Engineering, 2021, 8(1); 254-267.

u makaleye atıf yapmak için

Kati, M. İ., Keskin, İ.Ç., Türemiş, M., Çetin, A., Kibar, R. "Sol-Jel Tekniği ile Sentezlenmiş Sr_{0,5}Ca_{0,5}WO₄ Fosforunda Eu³⁺ İyonunun Lüminesans, TL Kinetik Parametreler ve Elektrokimyasal Davranışındaki Rolü", El-Cezeri Fen ve Mühendislik Dergisi 2021, 8(1); 254-267.

ORCID ID: *0000-0002-9225-730X; *0000-0003-2743-766X; *0000-0001-8849-4364; *0000-0003-4453-1906; *0000-0002-4183-9406

1. Introduction

Recently, studies on trivalent rare-earths (RE^{3+}) doped phosphors have increased significantly [1]. These phosphors are used widely in potential fields, such as lighting, display devices, fluorescent and phosphorescent materials for biological applications, white light-emitting diodes (WLEDs), sensors, and dose sensitivity improvements nuclear medicine field dating of biological samples, etc.[2]. WLEDs appear as light sources in various fields with economic advantages in repair and energy as well as positive benefits on the environment [3]

The tungstate and molybdate-based derivatives (ABO_4 : Ca^{2+} , Sr^{2+} , Ba^{2+} , $B:MO^{6+}$, W^{6+}) are appropriate host materials for the addition of trivalent lanthanide ions (RE^{3+}). New compounds formed by the combination of tetrahedral [VO_4 , PO_4 , MoO_4 , and WO_4] group are ideal host material for phosphors due to these clusters thermal and chemical stability [4]. The chemical stability of WO_4 is activated depending on the geometry, which has a central W metal ion that is coordinated by four O^{2-} in tetrahedral symmetry [5]. Rare-earths such as Eu^{3+} doped in tungstate are widely known as luminescent materials having unique chemical and physical properties [6]. The physical properties of these materials are based on lattice defects that occur folded by other ions. The difference in electronic density between the dopant and host material and the differences in electronic orientation structures are the most important factors for forming luminescence centers [7]. Generally, Eu^{3+} doped tungstate-based materials are expected to have characteristic red luminescence emission. This characteristic emission is based on the electronic orbital properties of materials [8]. These electronic properties are derived from the shape, size, crystal types, and compositions that rely on synthesis methods[9]. Many methods are used in the synthesis of inorganic substances, such as solid-state reactions, precursor polymeric, electrochemical cells [10], galvanic cells [11], molten salts [12], microwave, Pechini [13], Czochralski [14], co-precipitation [15], flame spray [16] and sol-gel [2]. The sol-gel method is of much interest due to its advantages, such as easy stoichiometric control, good homogeneity, and low calcination temperature. Besides, generally prepared materials by sol-gel process excellent luminescent properties and small particle size.

In this article, un-doped $Sr_{0.5}Ca_{0.5}WO_4$ and $Sr_{0.5-x}Ca_{0.5}WO_4:Eu_x^{3+}$ highly luminescent phosphors were prepared by the sol-gel method for the first time. The changes that occur with Eu^{3+} doping in the sample's optical, structural, and morphological properties were examined. For the first time, radioluminescence and photoluminescence properties of $Sr_{0.5}Ca_{0.5}WO_4:0.5Eu^{3+}$ (mol %) were investigated in detail. In addition to RL and PL measurements, TL glow curves of the samples were also taken. The RL system is different from PL due to its excitation source. Unlike the PL system, X-ray radiation penetrates the entire sample in the RL system to stimulate it and generate new luminescence defects [17]. In addition to these investigations, XRD, TG-DTA, absorption measurements, and SEM images of these phosphors were also taken and interpreted.

2. Materials and Methods

2.1.Preparation of Samples

2.1.1. Synthesis of $Sr_{0.5}Ca_{0.5}WO_4:Eu^{3+}$

All the chemicals used in this study were obtained from commercial suppliers. Europium (III) nitrate hydrate (Sigma Aldrich 99.9%) was used as the dopant rare earth material. As starting materials, Strontium nitrate ($Sr(NO_3)_2$) (Acros Organics 99+%), Calcium nitrate tetrahydrate ($Ca(NO_3)_2 \cdot 4H_2O$) (Sigma Aldrich 99.9%), Ammonium para tungstate ($(NH_4)_{10}H_2(W_2O_7)_6 \cdot xH_2O$) (Merck 99%), were used, and also citric acid monohydrate ($C_6H_8O_7 \cdot H_2O$) was utilized as a chelating agent. All aqueous solutions were prepared using double distilled. The number of materials to be

used was primarily calculated as 0.01 molar, taking into account stoichiometric coefficients. The ammonium para tungstate was fully dissolved in 300 ml of double-distilled water at 90 °C and was continuously mixed until it became transparent. The solution was allowed to cool at room temperature. No precipitate formed in the solution. The molar ratio (total metal cations: citric acid) was 1:3. Strontium nitrate and calcium nitrate tetrahydrate were dissolved together in another container, and then with continuous magnetic stirring at room temperature, 50 ml aqueous solution containing $(\text{NH}_4)_{10}\text{H}_2(\text{W}_2\text{O}_7)_6 \cdot x\text{H}_2\text{O}$ was slowly added to this solution. By dissolving in 10 ml of ionized water, the dopant (europium III nitrate hydrate) was added to this solution. The stirring time of the resulting solution was 2 h. The solution was kept in an oven for 16 hours at 80 °C. By evaporating water, a clear gel was obtained. The gel was dried in an oven at 120 °C for approximately 24 h. In order to remove the nitrate in the dry gel content, it was thoroughly dried by increasing it by 10 °C from 120 °C to 200 °C in 45-minute steps. Ultimately, via TG DTA analysis, the heat treatment process has been determined, and powder phosphor has been obtained using this process.

2.2. Characterization

X-ray diffraction (XRD) patterns of the prepared $\text{Sr}_{0.5}\text{Ca}_{0.5}\text{WO}_4:\text{Eu}^{3+}$ luminescent powders through sol-gel reaction technique were carried out under room temperature by a PANalytical Empyrean X-ray diffraction (XRD) appliance. The diffractometer's voltage and current values in this study were set to 45 kV and 40 mA, respectively. Cu-K α (1.5405 Å) was used as the radiation source. XRD patterns were obtained by step scanning from 10°-80° (2 θ in steps of 0.01313°; 59.925 s per step; 0.055 °/s scan speed and 5331 number of step). Before XRD measurements, all samples were kept in an oven at 90°C for 12 hours to remove possible ambient humidity and were cooled to room temperature in a desiccator.

TG-DTA measurements of phosphors samples were carried out synchronously employing Exstar S11 TG/DTA 7300 thermal analyzer. These measurements were studied in the temperature range of 25-1000 °C at a heating rate of 10 °C min⁻¹ in the argon atmosphere. By using Perkin-Elmer Lambda 950 spectrophotometer, the optical absorption spectra of samples were registered at room temperature in the wavelength region of 200–800 nm. It was not shown in the graph as there was no peak in part after 500 nm.

PL spectra were recorded using an FLS920 spectrofluorometer. Also, the photoluminescence instrument is equipped with a Standard xenon lamp (488 nm). The RL spectra were created in an X-ray unit with a Machlett OEG-50A tube running with a current of 15 mA and a voltage of 30 kV, delivering a dose rate of 30 Gy min⁻¹. The luminescence detection system is conducted with a Jobin Yvon spectrometer coupled to a liquid nitrogen cooled CCD detector.

The UV irradiated phosphors for TL analysis were readout in the darkroom with an RA94 Reader/Analyser system at a linear heating rate of 2 °C/s from 50 °C to 350 °C in an N₂ atmosphere in a dark environment.

The Nova Nano SEM 650 field-emission scanning electron microscope (FE-SEM) was utilized to investigate these phosphors' morphology. SE (secondary electron) detector was selected for SEM images, and the working distance (WD) was set to about 7mm. For host and doped phosphorus, images were taken at 10Kx and 20Kx magnifications.

A conventional three-electrode electrochemical system was used to investigate the electrochemical behavior of samples [18]. Cyclic voltammetry was performed on an Autolab potentiostat-galvanostat (PGSTAT 101 and PGSTAT 128N) with a three-electrode system. Three electrodes,

which consisted of a working electrode (having a 3mm diameter glassy carbon electrode), auxiliary electrode (a bright platinum wire), and a reference electrode (Ag/AgCl (sat. KCl)) were used in all measurements taken at room temperature.

3. Result and Discussion

3.1. Crystal Structure of $\text{Sr}_{0.5}\text{Ca}_{0.5}\text{WO}_4:\text{Eu}^{3+}$

Generally, the anticipated optimum crystallinity phosphors have stronger lighting and smaller traps. Besides, crystallization and phase structure are some of the important parameters for luminescent materials [19]. The crystallinity of the host $\text{Sr}_{0.5}\text{Ca}_{0.5}\text{WO}_4$ luminescent powder and its Eu^{3+} doped variety were examined by X-ray diffraction. Fig. 1 shows the XRD patterns of $\text{Sr}_{0.5}\text{Ca}_{0.5}\text{WO}_4$ and $\text{Sr}_{0.5}\text{Ca}_{0.5}\text{WO}_4:0.5\text{Eu}^{3+}$ (mol %) prepared by the sol-gel method and sintered 2 hours at 900°C . Additionally, the XRD pattern of these materials is compared with the SrWO_4 given in the literature (ICSD card number 98-015-5745). As it can be seen, all of the phases of the phosphorus synthesized can be indexed as tetragonal scheelite phase (space group: $I41/a$ and group number:88), and it is compatible with the literature [20]. Lattice and structural parameters of $\text{Sr}_{0.5}\text{Ca}_{0.5}\text{WO}_4$ (Table 1.) were calculated with the Rietveld refinement using the High Score Plus program. The lattice parameters were found to $d=2.9211\text{\AA}$, $a= 5.3316\text{\AA}$, $b= 5.3316\text{\AA}$, $c= 11.6844\text{\AA}$ for tempered $\text{Sr}_{0.5}\text{Ca}_{0.5}\text{WO}_4$ sample (represented Fig. 2).

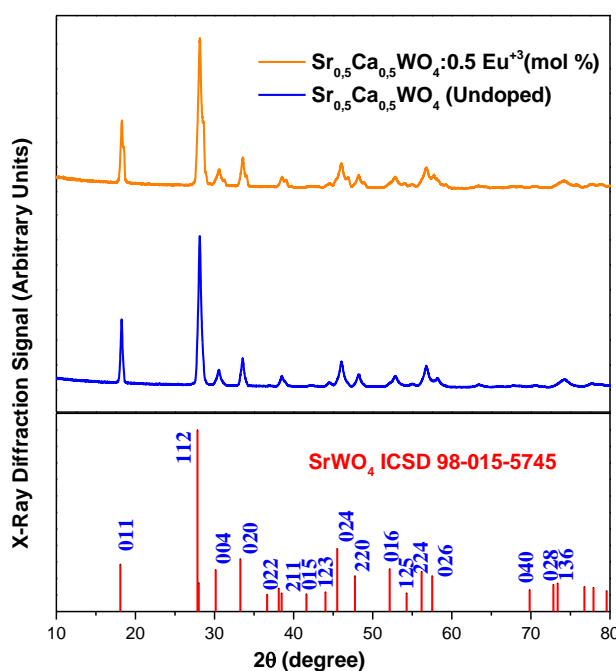


Figure 1. XRD patterns of the $\text{Sr}_{0.5}\text{Ca}_{0.5}\text{WO}_4$ and $\text{Sr}_{0.5}\text{Ca}_{0.5}\text{WO}_4:\text{Eu}^{3+}_{0.05}$ compared with the standard data of SrWO_4

Some rare-earth ions like Tb^{3+} , Eu^{3+} are susceptible in $\text{Sr}_{0.5}\text{Ca}_{0.5}\text{WO}_4$ crystal lattice, and the Eu^{3+} -dope does not significantly affect the phase structure. Moreover, XRD patterns revealed the lack of diffraction peaks attributed to the europium oxide (Eu_2O_3) and (CaO) that proposes to $\text{Sr}_{0.5}\text{Ca}_{0.5}\text{WO}_4:\text{Eu}^{3+}$ phosphors were produced in their pure state. The average crystallite size was found to 57 nm, 59 nm for un-doped $\text{Sr}_{0.5}\text{Ca}_{0.5}\text{WO}_4$ and $\text{Sr}_{0.5}\text{Ca}_{0.5}\text{WO}_4:0.5\text{Eu}^{3+}$ (mol %) respectively.

The crystallite size was calculated using Debye-Scherrer's formula from the plane (112), the highest peak of the XRD model; $D = k\lambda/\beta\cos\theta$, where D is the crystallite size (nm), $k=0.94$, $\lambda_{\text{Cu}}=0.15406$ nm, β is the full-width at half-maximum of the peak in radians corrected from instrumental broadening, θ is peak angle.

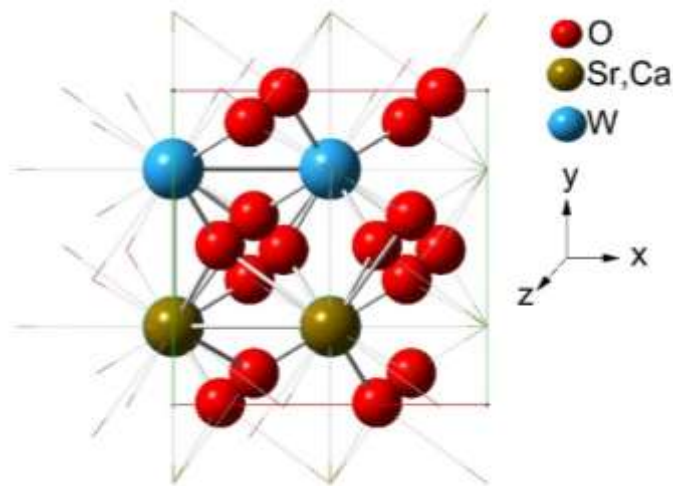


Figure 2. Representative tetragonal scheelite structure of $\text{Sr}_{0.5}\text{Ca}_{0.5}\text{WO}_4$

Table 1. The lattice parameters of un-doped $\text{Sr}_{0.5}\text{Ca}_{0.5}\text{WO}_4$ and $\text{Sr}_{0.5}\text{Ca}_{0.5}\text{WO}_4:\text{Eu}^{3+}$ phosphors.

Samples	(hkl)	$2\theta(^{\circ})$	$d(\text{\AA})$	$a(\text{\AA})$	$b(\text{\AA})$	$c(\text{\AA})$	Volume of cell (10^6pm^3)
ICSD#98-015-5745	(004)	30.153	2.9615	-	-	11.8460	343.26
	(020)	33.261	2.6915	5.3830	5.3830	-	
Un-Doped $\text{Sr}_{0.5}\text{Ca}_{0.5}\text{WO}_4$	(004)	30.578	2.9211	-	-	11.6844	332.14
	(020)	33.590	2.6658	5.3316	5.3316	-	
$\text{Sr}_{0.45}\text{Ca}_{0.5}\text{WO}_4:\text{Eu}^{3+}_{0.05}$	(004)	30.542	2.9246	-	-	11.6984	333.81
	(020)	33.523	2.6710	5.3418	5.3418	-	

3.2. Thermal Properties of $\text{Sr}_{0.45}\text{Ca}_{0.5}\text{WO}_4:\text{Eu}^{3+}_{0.05}$

For phosphors used in white emitting LEDs, thermal properties are critical technological parameters. Therefore, TG-DTA analyses were performed to understand the thermal properties of $\text{Sr}_{0.5}\text{Ca}_{0.5}\text{WO}_4$ phosphor. The powder sample produced by the sol-gel method and dried after the gelation process was prepared to decide the path to be followed in the heat treatment technique. Exstar brand S11 TG/DTA 7300 model device was used to determine the thermal properties and the appropriate heat treatment regime. The measurement was carried out in an argon atmosphere. The sample was heated up to 1000°C , and the heating rate was $10^{\circ}\text{C}/\text{min}$.

Figure 3 shows the thermal behavior of the dried gel of $\text{Sr}_{0.5}\text{Ca}_{0.5}\text{WO}_4$ precursor solution. It is seen that 50 % weight of dried gel was lost at the end of the thermal analysis. The reason for this is that the precursor solutions include a massive amount of organic compounds. This is the typical characteristic of the sol-gel technique [21]. Firstly the solution was dried at 200°C , and solvent molecules have left the structure. So that reactions started after 200°C in thermal analysis. Progress of weight loss continued from the temperature of 200°C to 850°C . The endothermic peak after 200°C might be the related decomposition of excess non-chelated citric acid [22].

DTA curve shows several exothermic peaks between 300 and 600 °C. These peaks at about 320, 410, and 520 °C correspond to the pyrolysis of organic compounds. A sharp endothermic peak located around 820 °C indicated the crystallization of the gel [11].

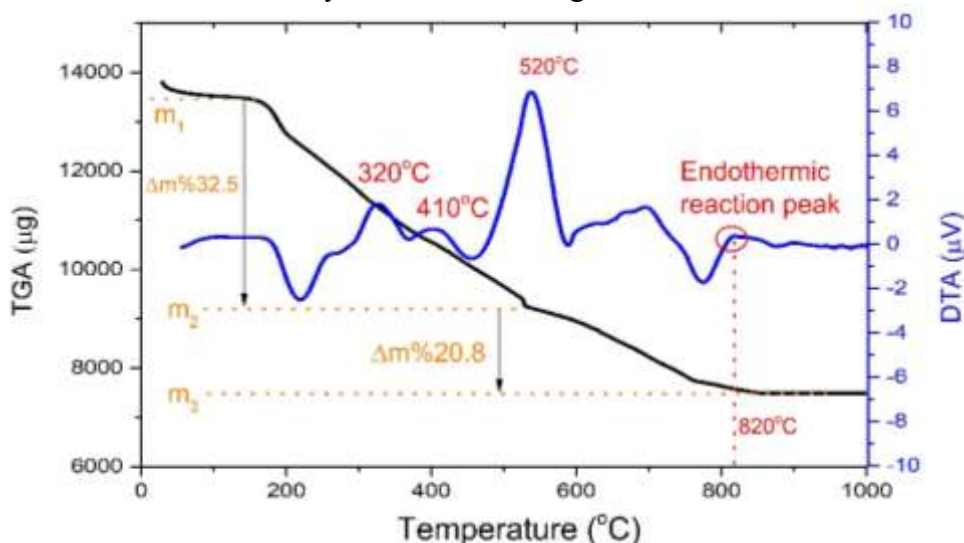


Figure 3. DTA and TGA graph of the $Sr_{0.5}Ca_{0.5}WO_4$

The heat treatment regime to synthesize the desired phase was determined in the light of thermal analysis results. The $Sr_{0.5}Ca_{0.5}WO_4$ and $Sr_{0.5}Ca_{0.5}WO_4:0.5Eu^{3+}$ (mol %) phosphors which are prepared by the sol-gel method sintered 2 hours at 900°C.

3.3. FT-IR Results

FT-IR spectra of the samples taken in the range of 450-4000 cm^{-1} are shown in Fig.4. The FT-IR research was applied to total qualitative information about the principal components in the samples. When generally looking in Fig.4, both samples showed similar spectral bands.

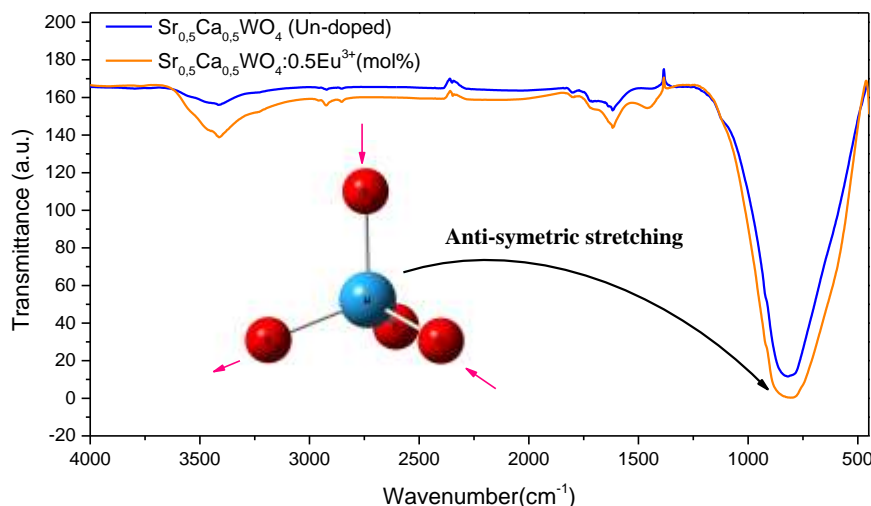


Figure 1. The FT-IR spectrum of the $Sr_{0.5}Ca_{0.5}WO_4$ and $Sr_{0.45}Ca_{0.5}WO_4:Eu^{3+}_{0.05}$

For both samples, the reasonably wide absorption band, which has a peak at 3400 cm^{-1} and extending to the wavenumber range to 3100 cm^{-1} , is assigned to the O-H stretching of H_2O on the surface of the samples. The peaks around 2400 cm^{-1} are thought to be caused by C-O vibrations of

atmospheric CO_2 [23]. In the region of $500\text{-}1000\text{ cm}^{-1}$ in the FT-IR spectrum of the $\text{Sr}_{0,5}\text{Ca}_{0,5}\text{WO}_4$ and $\text{Sr}_{0,5}\text{Ca}_{0,5}\text{WO}_4:0.5\text{Eu}^{3+}$ (mol%) samples, the spectra show a characteristic band of W-O anti-symmetric stretching vibration in $[\text{WO}_4]^{2-}$ tetrahedrons at $750\text{-}910\text{ cm}^{-1}$. This band is one of the internal modes specified as $\nu_3(\text{F}_2)$ anti-symmetric stretching vibration, and FT-IR results are appropriate with other MWO_4 ($\text{M}=\text{Ba}$, Sr , and Ca) in the literature[24].

3.4. Morphological Properties of Phosphors

The FE-SEM also investigated the morphology of the host and doped phosphors. It can be seen clearly from the images(Fig. 5); the dopant ions show good uniformity. The $\text{Sr}_{0,45}\text{Ca}_{0,5}\text{WO}_4:\text{Eu}^{3+}_{0,05}$ samples were composed through a soft chemical process in which Eu^{3+} , Sr^{2+} , Ca^{2+} , and WO_4^{2-} ions were homogeneously mixed in molecular levels.

The host material $\text{Sr}_{0,5}\text{Ca}_{0,5}\text{WO}_4$ has a tetragonal crystal structure as determined in the XRD analysis. Besides, in doped phosphors, SEM image Fig.5 (c-d) showed that the morphology was relatively spheroid. These structures are formed by Eu^{3+} contribution.

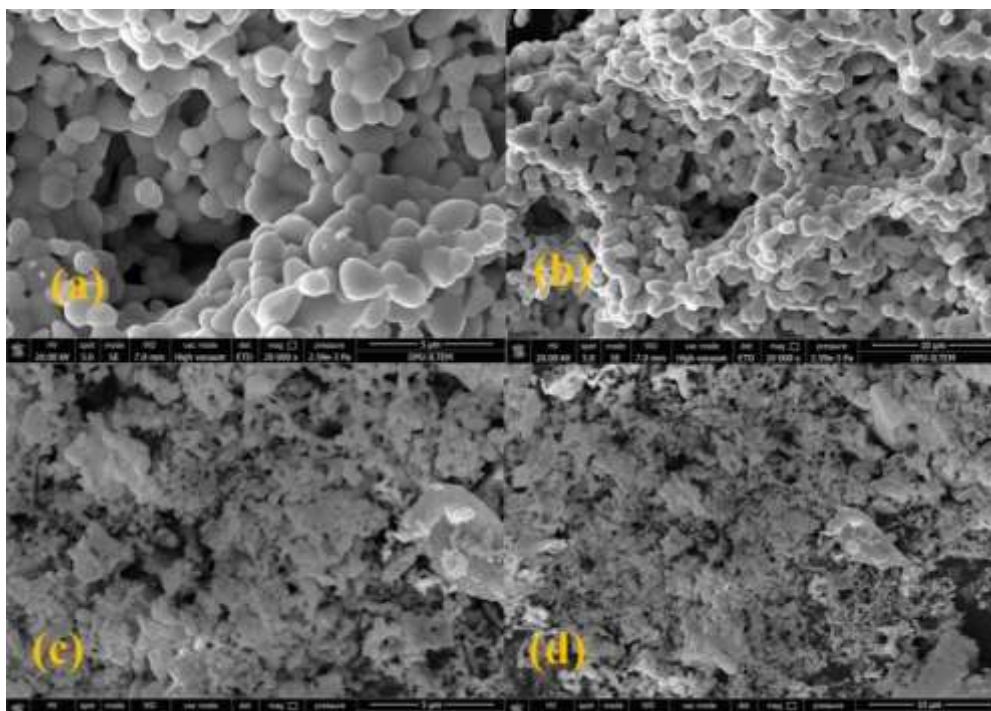


Figure 2. SEM images of un-doped $\text{Sr}_{0,5}\text{Ca}_{0,5}\text{WO}_4$ (a-b), $\text{Sr}_{0,5}\text{Ca}_{0,5}\text{WO}_4:0.5\text{Eu}^{3+}$ (mol %) (c-d).

3.5. Optical Properties of Host and $\text{Sr}_{0,45}\text{Ca}_{0,5}\text{WO}_4:\text{Eu}^{3+}_{0,05}$

The dopant effect on the luminescent properties and emission spectra of $\text{Sr}_{0,5}\text{Ca}_{0,5}\text{WO}_4$ were investigated with different excitation sources. The spectra were obtained for the phosphor materials as a result of X-ray stimulation in the RL system and light stimulation in the PL system, and those are indicated in Fig. 6 and Fig. 7. The RL spectra were recorded at room temperature for un-doped and Eu^{3+} doped $\text{Sr}_{0,5}\text{Ca}_{0,5}\text{WO}_4$ phosphors synthesized by the sol-gel method under X-ray irradiation. Figure 6a shows the RL spectrum of un-doped $\text{Sr}_{0,5}\text{Ca}_{0,5}\text{WO}_4$ range from 300 to 900 nm at room temperature. A broad emission of 350-750 nm appears in the RL spectrum of the host material. When this emission is examined in detail, wavelengths of peaks are approximately 420, 464, 506, and 526 nm. It can be said that the radiative transitions cause it within WO_4^{2-} complexes, creating charge transfer from O to W ions in the host material [25]. This quite strong emission continues to

exist after the Eu contribution. As can be seen that, the RL spectra line of Eu^{3+} ion contains sharp emission peaks between 550 and 750 nm (Fig. 6b), which are derived from the electronic transitions of ${}^5\text{D}_0 \rightarrow {}^7\text{F}_j$ ($J=1, 2, 3, 4$). When the crystal cage is doped with Eu^{3+} , the broad emission band in the range of 400-700 nm is significantly reduced, and the characteristic emission peaks of Eu^{3+} are improved. These emission peaks are clear evidence for energy transfer from the host material (Undoped $\text{Sr}_{0.5}\text{Ca}_{0.5}\text{WO}_4$) to Eu^{3+} . Also, the transition lines of host material $\text{Sr}_{0.5}\text{Ca}_{0.5}\text{WO}_4$, which is doped with Eu^{3+} (592 nm, ${}^5\text{D}_0 \rightarrow {}^7\text{F}_1$; 614 nm, ${}^5\text{D}_0 \rightarrow {}^7\text{F}_2$; 650 nm, ${}^5\text{D}_0 \rightarrow {}^7\text{F}_3$; 700 nm, ${}^5\text{D}_0 \rightarrow {}^7\text{F}_4$) are seen in the RL and PL emission spectra. At the same time, the absorption bands (${}^7\text{F}_0 \rightarrow {}^5\text{G}_5$, ${}^7\text{F}_0 \rightarrow {}^5\text{F}_2$, ${}^7\text{F}_0 \rightarrow {}^5\text{L}_7$, ${}^7\text{F}_0 \rightarrow {}^5\text{D}_4$, ${}^7\text{F}_0 \rightarrow {}^5\text{L}_6$, ${}^7\text{F}_0 \rightarrow {}^5\text{D}_3$, ${}^7\text{F}_0 \rightarrow {}^5\text{D}_2$, ${}^7\text{F}_0 \rightarrow {}^5\text{D}_1$ transitions) are observed for $\text{Sr}_{0.45}\text{Ca}_{0.5}\text{WO}_4:\text{Eu}^{3+}_{0.05}$; in the PL excitation spectrum (Fig. 7 b). The red light is caused by ${}^5\text{D}_0 \rightarrow {}^7\text{F}_2$ electric-dipole transition of Eu^{3+} . The ${}^5\text{D}_0 \rightarrow {}^7\text{F}_2$ transition strongly influenced by the chemical environment of Eu^{3+} in the host lattice is stronger than the transition of ${}^7\text{F}_1$ energy level, which indicates Eu^{3+} in low symmetry fields [2]. If the Eu ions occupy sites without an inversion center (i.e., low symmetry sites), electrical dipole transitions are evident [26]. The transition: ${}^5\text{D}_0 \rightarrow {}^7\text{F}_1$, at 592 nm, originates from the parity-allowed magnetic dipole transition and is non-sensitive to the crystal field environment. This transition becomes prominent for the cases when Eu ions are located at high symmetry sites. The higher intensity of electric dipolar transitions (614 nm) than magnetic dipolar transitions (592 nm) shows that Eu ions in $\text{Sr}_{0.5}\text{Ca}_{0.5}\text{WO}_4$ lattice are located at low symmetry sites.

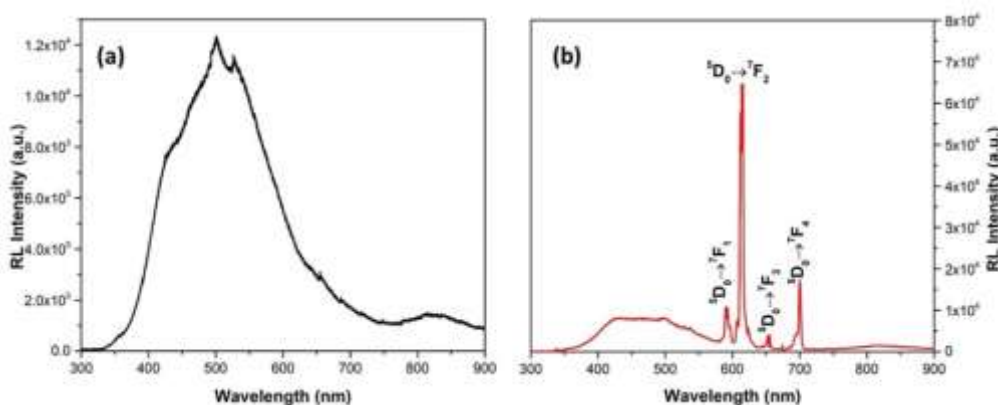


Figure 3. RL spectra of un-doped $\text{Sr}_{0.5}\text{Ca}_{0.5}\text{WO}_4$ (a) and $\text{Sr}_{0.5}\text{Ca}_{0.5}\text{WO}_4:0.5\text{Eu}^{3+}$ (mol %)(b).

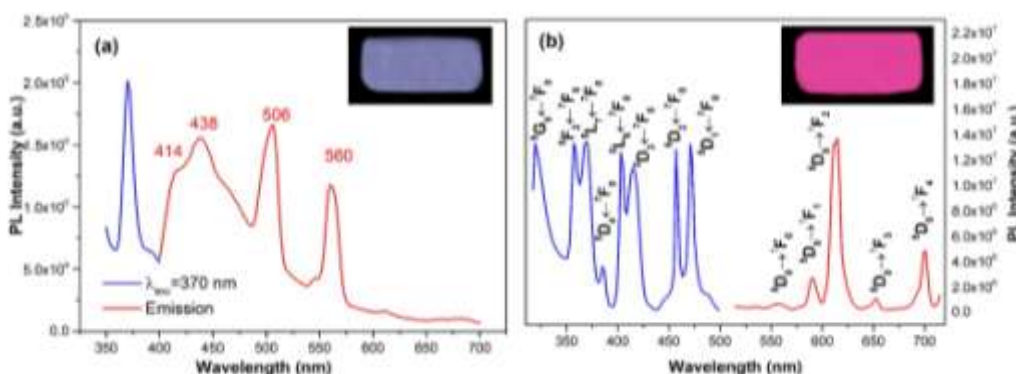


Figure 4. Photoluminescence excitation and emission spectra of un-doped $\text{Sr}_{0.5}\text{Ca}_{0.5}\text{WO}_4$ (a) and $\text{Sr}_{0.5}\text{Ca}_{0.5}\text{WO}_4:0.5\text{Eu}^{3+}$ (mol%)(b).

Figure 7a. shows the PL excitation and emission spectrum of un-doped $\text{Sr}_{0.5}\text{Ca}_{0.5}\text{WO}_4$ range from 350 to 700 nm at room temperature. When the sample is excited under 370 nm light, $\text{Sr}_{0.5}\text{Ca}_{0.5}\text{WO}_4$ emits a broad emission in the electromagnetic spectrum's blue region resulting from W-O charge transitions within $[\text{WO}_4]^{2-}$ group and peaking at 414, 438, 506, and 560 nm. In summary, it was

observed that there are broad emission bands in the visible region in both RL and PL spectra for un-doped $\text{Sr}_{0.5}\text{Ca}_{0.5}\text{WO}_4$. This situation is not often observed. So the emission spectra of RL and PL represent that Eu^{3+} doped $\text{Sr}_{0.5}\text{Ca}_{0.5}\text{WO}_4$ can be used as a red phosphor for LEDs.

3.6. Thermoluminescence (TL) Properties

The thermoluminescence (TL) glow curves for un-doped, and doped phosphors at a heating rate of $2\text{ }^\circ\text{C}\cdot\text{s}^{-1}$ are shown in Fig. 8. TL glow curves were obtained after 10 min short-wave UV (254 nm) irradiation in the darkroom. As shown in Fig. 8, TL glow curves at 90 and 250 $^\circ\text{C}$, which have a shoulder at around 202 $^\circ\text{C}$, have been observed for un-doped $\text{Sr}_{0.5}\text{Ca}_{0.5}\text{WO}_4$. Three main glow peaks have been observed for $\text{Sr}_{0.45}\text{Ca}_{0.5}\text{WO}_4:\text{Eu}^{3+}_{0.05}$; the first (55 $^\circ\text{C}$) and second (145 $^\circ\text{C}$) broad peaks include the peaks of the host material; the third one is at 215 $^\circ\text{C}$ with a shoulder at around 175 $^\circ\text{C}$. The traps formed by Eu^{3+} ion doping in the crystal lattice resulted in the TL curves at high temperatures. These TL spectra are very complex and difficult to interpret. In interpreting the TL spectra, there are many parameters such as the variety of excitation sources, the energy level of stimulation source, and the excitation of deep and shallow traps close to the recombination center. Therefore, the deconvolution of complex glow curves into their components is widely applied for evaluating the kinetic parameters using curve fitting methods [27,28].

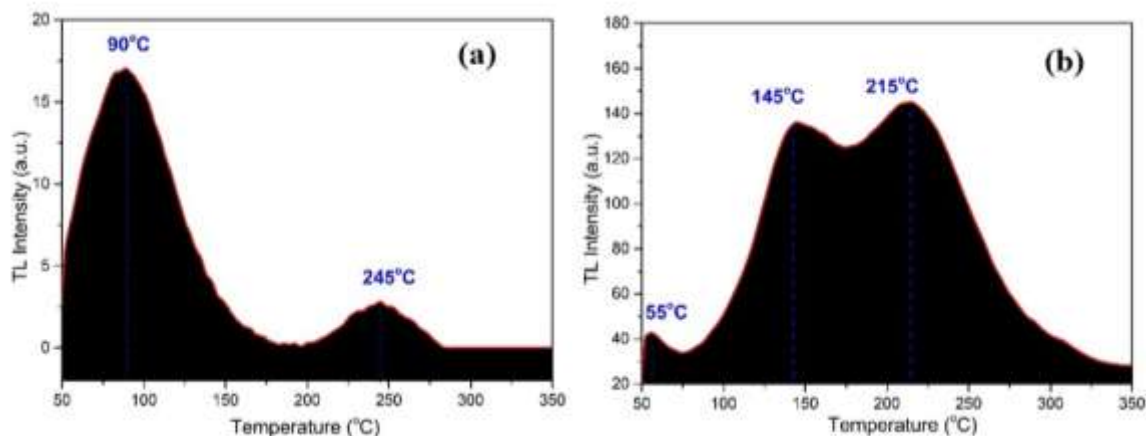


Figure 5. TL glow curves of $\text{Sr}_{0.5}\text{Ca}_{0.5}\text{WO}_4$ (a) and $\text{Sr}_{0.5}\text{Ca}_{0.5}\text{WO}_4:0.5\text{Eu}^{3+}$ (b) under 10 min. UV irradiation (254nm).

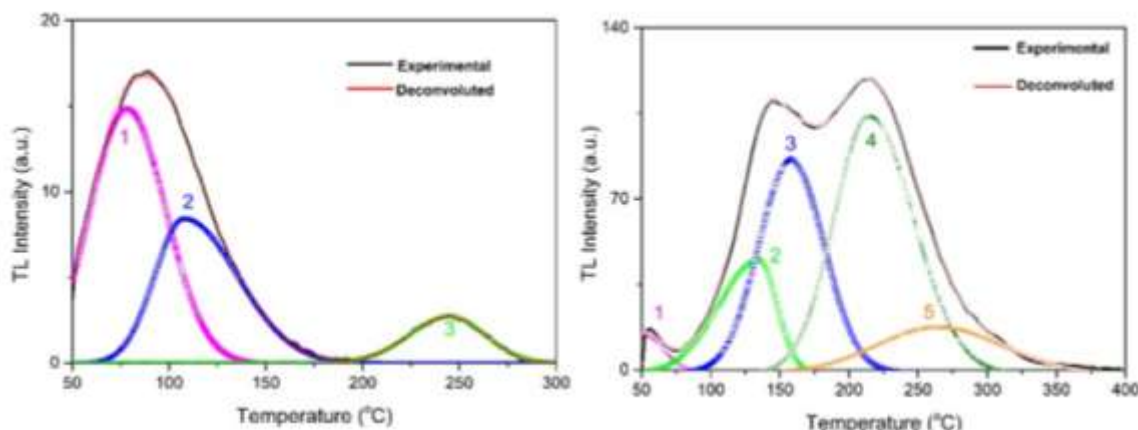


Figure 6. Fitted multiparameter peaks for main TL glow curves.

Computerized glow curve deconvolution (CGCD) analysis was performed to separate each peak from the main TL glow curve. As seen from Fig. 9, the analyzed TL glow curves occurred three and five glow peaks for un-doped $\text{Sr}_{0.5}\text{Ca}_{0.5}\text{WO}_4$ and $\text{Sr}_{0.5}\text{Ca}_{0.5}\text{WO}_4:\text{Eu}^{3+}_{0.05}$, respectively. The analysis of the peak maxima was solved with high accuracy ($r^2 = 0.996$ and 0.998). The kinetic parameters of

these peaks are given in Table 2. The calculated activation energy and frequency factor values are in harmony with each other.

Table 2. Physical parameters obtained from the deconvolution of TL glow curves of Un-doped and (0,5 mol%)Eu³⁺ doped Sr_{0,5}Ca_{0,5}WO₄ (Fig. 9) with r² = 0.996 and 0.998 respectively. (I_m: the intensity of the peak maxima, T_m (°C): Temperature of the peak maxima, E (eV): The activation energy, s(s⁻¹): The frequency factor, μ: The kinetic order)

	Peak Number	I _m	T _m (°C)	E (eV)	s(s ⁻¹)	μ
Un-Doped Sr _{0,5} Ca _{0,5} WO ₄	1	14.843	78.2	0.744±0.006	6.65x10 ⁹	0.507
	2	8.417	107.8	1.221±0.018	2.82x10 ¹⁵	0.660
	3	2.695	244.9	1.463±0.006	2.18x10 ¹³	0.478
Sr _{0,45} Ca _{0,5} WO ₄ : Eu ³⁺ _{0,05}	1	14.81	50.4	0.860±0.002	5.00x10 ¹²	0.503
	2	44.91	134.7	1.282±0.004	1.35x10 ¹⁵	0.461
	3	85.94	157.9	0.916±0.011	5.92 x10 ⁹	0.501
	4	103.65	214.5	1.118±0.021	3.95 x10 ¹⁰	0.553
	5	17.51	264.7	0.749±0.032	6.30 x10 ¹¹	0.505

3.7. Optical Properties

Figure 10 shows optical absorption spectra (in the 200-800 nm range) of un-doped and Eu³⁺ Sr_{0,5}Ca_{0,5}WO₄ at room temperature and in the darkroom. The optical band gap measurement involves the excitation of electrons from the valance band to the conduction band using photons of selected frequencies. The process does not change the number of carriers involved, and the total numbers of carriers present in the semiconductor remain the same. The optical band gap (E_g) values were calculated the Tauc's equation αhv = (hv-E_g)ⁿ equation, where α represents the absorbance, h is the Planck's constant, v is the frequency, E_g is the optical energy gap, and n is a number associated with the type of electronic transitions[29].

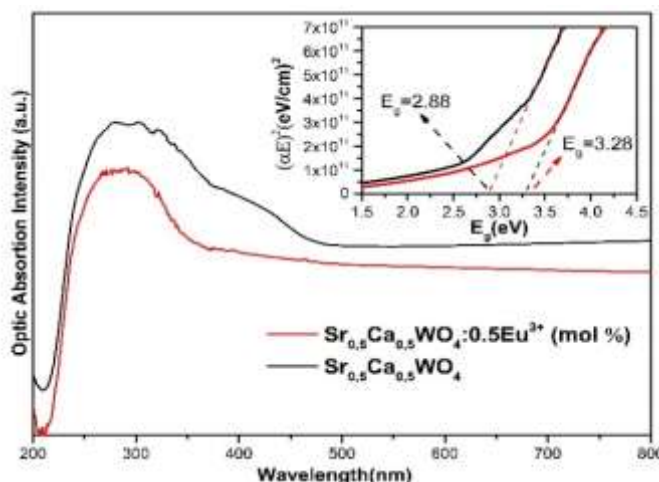


Figure 7. The optical absorption spectra and Tauc plot (inset) used calculating the bandgap of host Sr_{0,5}Ca_{0,5}WO₄ and Sr_{0,5}Ca_{0,5}WO₄:0.5Eu³⁺(% mol) phosphors.

From Fig. 10, the optical band gap of Sr_{0,5}Ca_{0,5}WO₄ was calculated as 2.88 eV. A significant change in the bandgap was observed by doping the Eu³⁺ ion to Sr_{0,5}Ca_{0,5}WO₄. The absorption band of Sr_{0,45}Ca_{0,5}WO₄:Eu³⁺_{0,05} phosphorus shifted to about 50 nm red region relative to the host material.

The energy band gap value of $\text{Sr}_{0.45}\text{Ca}_{0.5}\text{WO}_4:\text{Eu}^{3+}_{0.05}$ phosphorus increased to about 3.28 eV. Increasing structural defects with the RE^{3+} ion contribution causes localized states to occur in the energy band gap, which leads to an increase in the energy bandgap. The bandgap narrowing can be correlated with the strong s-d and p-d spin-exchange interactions between band electrons and localized d orbital electrons of Sr^{2+} ions in which Eu^{3+} ions occupy. The change in optical band gap can be attributed to electron-electron and electron-impurity scattering within the host and doped material [30]. It is seen that the optical absorption spectra of the samples are compatible with the PL excitation values.

3.8. Optical Visual Properties

It is seen that while the $\text{Sr}_{0.5}\text{Ca}_{0.5}\text{WO}_4$ host material was emitting bluish-white light, thanks to Eu^{3+} doping, the phosphor began to emit fuchsia light under a 254 nm UV lamp. This color change is an essential optical visibility phenomenon; energy transfer from the host material to rare-earth ions [31]. In Fig. 11, the CIE (1931) diagram of the un-doped and Eu^{3+} doped $\text{Sr}_{0.5}\text{Ca}_{0.5}\text{WO}_4$ powders was demonstrated with chromatic coordinates. The CIE coordinates of phosphors and their images were found to be compatible.

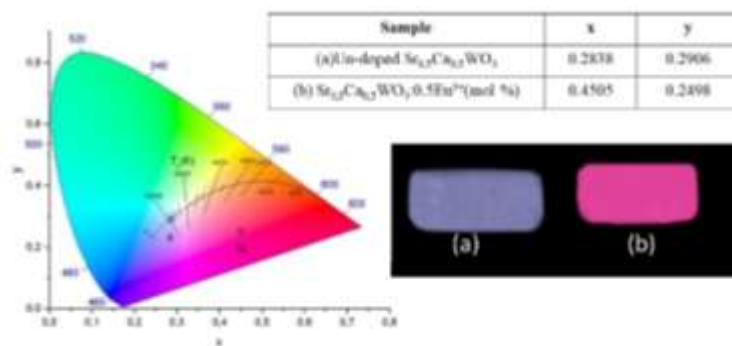


Figure 8. CIE diagram of the samples upon excitation at 370 nm and image of the phosphors when excited at 254 nm under a UV lamp in the darkroom.

3.9. Electrochemical Results

Cyclic voltammograms were carried out in the 1.5 M citric acid solution (pH 4.2) for investigated electrochemical properties of un-doped $\text{Sr}_{0.5}\text{Ca}_{0.5}\text{WO}_4$ and $\text{Sr}_{0.45}\text{Ca}_{0.5}\text{WO}_4:\text{Eu}^{3+}_{0.05}$ samples.

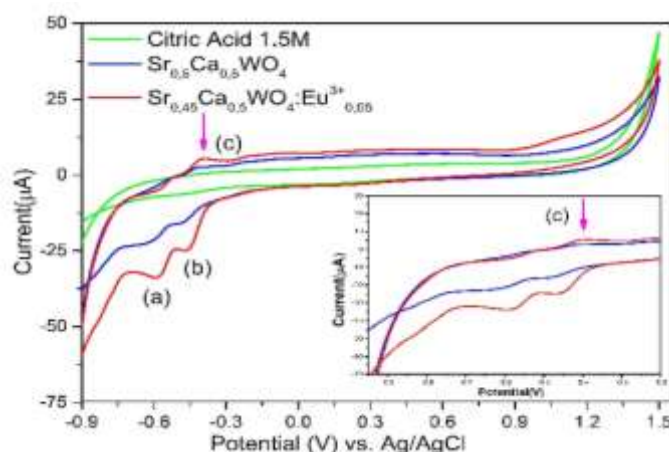


Figure 9. Cyclic voltammograms of un-doped $\text{Sr}_{0.5}\text{Ca}_{0.5}\text{WO}_4$ and $\text{Sr}_{0.5}\text{Ca}_{0.5}\text{WO}_4:\text{Eu}^{3+}$ in 1.5 M citric acid solution.

The applied potential was changed from -1 V to +1.5 V, and voltammograms were created from the current signals corresponding to these potentials. In Figure 12, shows cyclic voltammograms of Un-doped $\text{Sr}_{0.5}\text{Ca}_{0.5}\text{WO}_4$ and $\text{Sr}_{0.45}\text{Ca}_{0.5}\text{WO}_4:\text{Eu}^{3+}_{0.05}$ in 1.5 M citric acid solution. While (a) and (b)

peaks are common for Un-doped $\text{Sr}_{0,5}\text{Ca}_{0,5}\text{WO}_4$ and $\text{Sr}_{0,45}\text{Ca}_{0,5}\text{WO}_4:\text{Eu}^{3+}_{0,05}$ in these voltammograms, the (c) peak is only seen at $\text{Sr}_{0,45}\text{Ca}_{0,5}\text{WO}_4:\text{Eu}^{3+}_{0,05}$. It is thought to be the oxidation peak of the Eu ion.

4. Conclusion

In summary, un-doped and Eu^{3+} doped $\text{Sr}_{0,5}\text{Ca}_{0,5}\text{WO}_4$ phosphors were successfully synthesized by sol-gel technique (new host material), and also, RL behavior of these luminescent powders observed for the first time. XRD patterns determined phase structure, and no impurity phase was found in $\text{Sr}_{0,5}\text{Ca}_{0,5}\text{WO}_4$, $\text{Sr}_{0,5}\text{Ca}_{0,5}\text{WO}_4:0.5\text{Eu}^{3+}$ (mol%) phosphorus. The results present that the powder samples are tetragonal scheelite phase structures (space number: I41/a). The average crystallite size was found to 57 nm and 59 nm for host and $\text{Sr}_{0,5}\text{Ca}_{0,5}\text{WO}_4:0.5\text{Eu}^{3+}$ (mol%), respectively. As can be seen, (Fig. 5), the samples have a relatively spheroid morphology. When RL and PL measurements are examined in detail, common transitions (592 nm, $^5\text{D}_0 \rightarrow ^7\text{F}_1$; 614 nm, $^5\text{D}_0 \rightarrow ^7\text{F}_2$; 650 nm, $^5\text{D}_0 \rightarrow ^7\text{F}_3$; 700 nm, $^5\text{D}_0 \rightarrow ^7\text{F}_4$) were observed in both spectra for $\text{Sr}_{0,5}\text{Ca}_{0,5}\text{WO}_4:0.5\text{Eu}^{3+}$ (mol%). Three and five estimated glow peaks under main TL glow curves. The calculated kinetic parameters results are compatible. The bandgap value of the doped host sample was found to higher than the un-doped $\text{Sr}_{0,5}\text{Ca}_{0,5}\text{WO}_4$. The Eu^{3+} doped $\text{Sr}_{0,5}\text{Ca}_{0,5}\text{WO}_4$ phosphorus showed fuchsia luminescence, while the host material has turquoise emission under 254 nm UV lamp. From the cyclic voltammograms, data were obtained to demonstrate that Eu ions doped to host material. In light of this information, both in terms of energy transfer mechanism and color scale, $\text{Sr}_{0,45}\text{Ca}_{0,5}\text{WO}_4:\text{Eu}^{3+}_{0,05}$ may be used for optical-electronic applications, solid-state lighting, and a light-emitting diode.

Acknowledgment

The authors would like to thanks Manisa Celal Bayar University, Experimental Science Applications and Research Center (DEFAM) for the measurements taken in this study.

References

- [1]. Peközülü, İ., Erdoğmuş, E., Yılmaz, M., Synthesis and photoluminescence properties of $\text{Li}_4\text{SrCa}(\text{SiO}_4)_2: \text{M}$ (M: Pb^{2+} and Bi^{3+}), *Journal of Luminescence*, 2015, 161:160–163.
- [2]. Keskin, İ.Ç., Gültekin, S., Katı, M.İ., Türemiş M., Ay, K., Arslanlar, Y., Çetin, A., Kibar, R., Structural, optical, luminescence properties and energy transfer mechanism of $\text{Tb}^{3+}/\text{Eu}^{3+}$ co-doped $\text{SrLa}_2(\text{MoO}_4)_4$ phosphors produced by sol-gel process, *Journal of Alloys Compounds*, 2019, 789:932–940.
- [3]. Su, Y., Li, L., Li, G., Synthesis and Optimum Luminescence of CaWO_4 -Based Red Phosphors with Codoping of Eu^{3+} and Na^+ , *Chemistry and Materials*, 2008, 20:6060–6067.
- [4]. He, X., Guan, M., Lian, N., Sun, J., Shang, T., Synthesis and luminescence characteristics of $\text{K}_2\text{Bi}(\text{PO}_4)(\text{MO}_4):\text{Eu}^{3+}$ (M = Mo, W) red-emitting phosphor for white LEDs, *Journal of Alloys Compounds*, 2010, 492:452–455.
- [5]. Cao, F., Tian, Y., Chen, Y., Xiao, L., Wu, Q., Novel red phosphors for solid-state lighting: $\text{Ca}_{0,54}\text{Sr}_{0,34-1,5x}\text{Eu}_{0,08}\text{La}_x (\text{MoO}_4)_y(\text{WO}_4)_{1-y}$, *Journal of Alloys Compounds*, 2009, 475:387–390.
- [6]. Lei, F., Yan, B., Morphology-Controlled Synthesis, Physical Characterization, and Photoluminescence of Novel Self-Assembled Pomponlike White Light Phosphor: Eu^{3+} -Doped Sodium Gadolinium Tungstate, *Journal of Physics and Chemistry C*, 2009, 113:1074–1082.
- [7]. Jia, G., Wang, C., Xu, S., Local Site Symmetry Determination of Scheelite-Type Structures

- by Eu³⁺ Spectroscopy, *Journal of Physics and Chemistry C*, 2010, 114:17905–17913.
- [8]. Liao, j., You, H., Zhang, S., Jiang, J., Qiu, B., Huang, H., Wen, H., Synthesis and luminescence properties of BaWO₄:Pr³⁺ microcrystal, *Journal Rare Earths*, 2011, 29:623–627.
- [9]. Haque, M.M., Lee, H.-I., Kim, D.-K., Luminescent properties of Eu³⁺-activated molybdate based novel red-emitting phosphors for LEDs, *Journal of Alloys Compounds*, 2009, 481:792–796.
- [10]. Koçak, S., Aslışen, B., Hydrazine oxidation at gold nanoparticles and poly(bromocresol purple) carbon nanotube modified glassy carbon electrode, *Sensors Actuators, B Chemistry*, 2014, 196: 610–618.
- [11]. Pereira, P.F.S., Nogueira, I.C., Longo, E., Nassar, E.J., Rosa, I.L.V., Cavalcante, L.S. Rietveld refinement and optical properties of SrWO₄:Eu³⁺ powders prepared by the non-hydrolytic sol-gel method, *Journal of Rare Earths*. 2015, 33:113–128
- [12]. Xie, Y., Yang, H., Zeng, K., Zhu, Y., Hu, J., Mao, Q., Liu, Q., Chen, H., Study on CO₂ gasification of biochar in molten salts: Reactivity and structure evolution, *Fuel*, 2019, 254:115-214.
- [13]. Reis, J. V., Pereira, T.C.P.T., Teles, H.A., França, AB, Bellido, J., Naves, D.A., Baston, F.L., Synthesis of CeNb₃O₉ perovskite by Pechini method, *Materials and Letters*, 2018, 227:261–263.
- [14]. Romčević, N., Stojanović, D., Romčević, M., Khokhlov, D.R., Far-infrared galvanomagnetic study of gallium doped Pb-Te, *Journal of Alloys Compounds*, 2008, 460:13-19.
- [15]. Aleshin, D.K., Mashkovtsev, M.A., Kuznetsova, Y.A., Rychkov, V.N., Zatsepin, A.F., Gordeev, E. V., Fabrication of (Y_{0.95}Eu_{0.05})₂O₃ phosphors with enhanced properties by coprecipitation of layered rare-earth hydroxide, *Journal of Alloys Compounds*, 2019, 217:465-472.
- [16]. Gültekin, S., Yıldırım, S., Yılmaz, O., Keskin, İ.Ç., Katı, M.İ., Çelik, E., Structural and optical properties of SrAl₂O₄: Eu²⁺/Dy³⁺ phosphors synthesized by flame spray pyrolysis technique, *Journal of Luminescence*, 2019, 206:59–69.
- [17]. Keskin, İ.Ç., Türemiş, M., Katı, M.İ., Kibar, R., Şirin, K., Çipiloğlu, M.A., Kuş, M., Büyükçelebi, S., Çetin, A., The radioluminescence and optical behaviour of nanocomposites with CdSeS quantum dot, *Journal of Luminescence*, 2017, 185:118-125.
- [18]. Aslışen, B., Koçak, Ç.C., Koçak, S., Electrochemical Determination of Sesamol in Foods by Square Wave Voltammetry at a Boron-Doped Diamond Electrode, *Analytical Letters*, 2020, 53:343–354.
- [19]. Yıldırım, S., Yurddaskal, M., Dikici, T., Aritman, I., Ertekin, K., Celik, E., Structural and luminescence properties of undoped, Nd³⁺ and Er³⁺ doped TiO₂ nanoparticles synthesized by flame spray pyrolysis method, *Ceramic International*, 2016, 42:10579–10586.
- [20]. Huang, Z., Nie, Z., Xie, M., Wang, Y., Li, D., Excellent optical thermometry based on upconversion emission in SrMoO₄:Er³⁺ phosphor, *Optic Materials Express*, 2017, 7:2404-2410.
- [21]. Çetin, A., Keskin, İ.Ç., Katı, M.İ., Türemiş, M., Taştekin, B., Çipiloğlu, M.A., Kibar, R., The Investigation of Kinetic Characterization of Sea Salt via Thermoluminescence Method, *Celal Bayar University Journal of Science*, 2017, 13:845-849.
- [22]. Han, Y., Wang, X., Li, S., Ma, X., Synthesis of terbium doped calcium phosphate nanocrystalline powders by citric acid sol-gel combustion method, *Journal of Sol-Gel Science Technology*, 2009, 49:125–129.
- [23]. Keskin, İ.Ç., Katı, M.İ., Türemiş, M., Gültekin, S., Üstün, S., Çetin, A., Kibar, R., X-ray irradiated thermo- and radioluminescence, structural and thermal characterization of septarian (powder&bulk) from Madagascar, *Optic Materials (Amst)*, 2018, 83:176–181.

- [24]. Thongtem, T., Phuruangrat, A., Thongtem, S., Preparation and characterization of nanocrystalline SrWO₄ using cyclic microwave radiation, *Current Applied Physics*, 2008, 8:189–197.
- [25]. Phuruangrat, A., Thongtem, T., Thongtem, S., Synthesis, characterisation and photoluminescence of nanocrystalline calcium tungstate, *Journal of Experimental Nanoscience*, 2010, 5:263–270.
- [26]. Zhang, Y., Abraha, A., Zhang, R., Shahbazyan, T., Fadavi, M., Heydari, E., Dai, Q., Luminescence properties of CaWO₄ and CaWO₄:Eu³⁺ nanostructures prepared at low temperature, *Optical Materials (Amst)*, 2018, 84:115–122.
- [27]. Kadı, M.İ., Sam, G., Keskin, İ.Ç., Türemiş, M., Çetin, A., Kibar, R., Pembe Spodümenin Termoluminesans Özelliklerinin İncelenmesi ve Kinetik Parametrelerinin Hesaplanması, *El-Cezeri Fen ve Mühendislik Derg*, 2016, 3:258–271.
- [28]. Kadı, M.İ., Kadiroğulları, K., Türemiş, M., Keskin, İ.Ç., Çetin, A., Kibar, R., The Investigation of Thermoluminescence Properties of Tooth Enamel, *El-Cezeri Fen ve Mühendislik Derg*, 2016, 3:297–303.
- [29]. Tauc, J., Optical properties and electronic structure of amorphous Ge and Si, *Materials Research Bullteın*, 1968, 3:37–46.
- [30]. Tirumalareddygarı, S.R., Guddeti, P.R., Ramakrishna, K., Reddy, T., A critical study of the optical and electrical properties of transparent and conductive Mo-doped ZnO films by adjustment of Mo concentration, *Applied Surface. Science*, 2018, 458:333–343.
- [31]. Mahalingam, V., Thirumalai, J., Krishnan, R., Mantha, S., Up/down conversion luminescence and charge compensation investigation of Ca_{0.5}Y_{1-x}(WO₄)₂:xLn³⁺ (Ln=Pr, Sm, Eu, Tb, Dy, Yb/Er) phosphors, *Spectrochimica. Acta Part A Moleculer. Biomoleculer. Spectroscopy*, 2016, 152:172–180.